IEEE Access
Multidisciplinary | Rapid Review | Open Access Journal

Received October 31, 2019, accepted November 18, 2019, date of publication November 22, 2019,
date of current version December 5, 2019.

*Digital Object Identifier 10.1109/ACCESS.2019.2955112*

# Multi-Objective Optimization of Solar/Wind Penetration in Power Generation Systems

**FARIHAN MOHAMAD, JIASHEN TEH, (Member, IEEE), AND HAMZA ABUNIMA**
School of Electrical and Electronic Engineering, Engineering Campus, Universiti Sains Malaysia (USM), Nibong Tebal 14300, Malaysia

Corresponding author: Jiashen Teh (jiashenteh@usm.my)

This work was supported in part by the Universiti Sains Malaysia (USM) Research University Incentive (RUI) under Grant 1001/PELECT/8014099, and in part by the Ministry of Education Malaysia Fundamental Research Grant Scheme (FRGS) under Grant 203/PELECT/6071442.

**ABSTRACT** Integrations of renewable energies, particularly solar and wind, are increasing worldwide due to carbon emission reduction efforts and maturing technologies that have driven down the cost of their energy productions. Due to the intermittency of these renewable sources, the battery energy storage system often coexists alongside solar/wind energy systems. Integrating these two aspects into power systems requires the consideration of reliability, social wellbeing and environmental factors, which collectively form a multi-objective optimization problem that this paper aims to solve with the non-dominated sorting genetic algorithm. The proposed method is able to find optimum solutions that are equally beneficial to all factors – Pareto front – without being heavily biased to any one of them. The proposed method is separated into two parts by first optimizing the penetration of solar/wind energy, followed by the optimization of the energy storage capacity in the second part. The fuzzy decision making method is utilized to select a preferred solution from the Pareto front based on the assignment of the membership function values to reflect operator's preferences. The proposed method was implemented on the IEEE Reliability Test System overlaid with the real sampled weather data. The proposed objectives in the optimization problem are also practical and useful for the expansion of generation systems.

**INDEX TERMS** Battery energy storage system, Monte Carlo simulation, reliability, solar energy, smart grid, wind energy.

## I. INTRODUCTION

The supply of energy is a critical part of sustainable development manifestation [1] and the power generation sector is constantly evolving to become more reliable while maintaining competitive operation costs without adversely impacting the wellbeing of society [2]. The term 'reliable' is defined as the ability of the generation system to adequately supply power to meet load demands [3], [4]. Hence, technical, economic and social aspects are the cornerstones of power network developments [5].

One of the strategies to achieve the sustainable production of energy is through the wide scale implementation of renewable energy (RE) sources as most of them have no carbon emission and they are therefore environmental friendly [6]. A main feature of the RE sources is its unlimited supply, but the downside risk is their intermittency property. Due to this, there are considerable concerns that question the ability of such a generation system to fill the energy gap caused by RE units during episodes of their intermittency. Hence, the common practice is to restrict the integration of RE within a certain percentage of system load to maintain system reliability [7]. However, this reduces the reliance on RE which contradicts the aim to minimize fossil fuel usage in power generation [8]. Consequently, technologies that are able to alleviate the intermittency problem of RE sources is needed and, studies have shown that the energy storage systems (ESSs) is able to store the extra energy produced during times of excesses for later usage [9]. Historically, ESSs were expensive and less deployed despite its ability, therefore other technologies such as the dynamic thermal rating system [10]–[16] and demand-side management [17]–[19] are more preferred. However, recent advancements have lowered the costs of ESSs and lead to its widespread adoption, subsequently increasing the penetration of RE [20]. Apart from the energy storing function, ESSs also need to

The associate editor coordinating the review of this manuscript and approving it for publication was Qiquan Qiao.

have fast response time so that mismatch between power generation and load demand is minimized [21]. In this regard, the battery ESS (BESS) satisfies this requirement very well owing to its high energy density characteristic. Moreover, it is also easier to be deployed than other types of ESS such as water dam, flywheel and etc., and this leads to its eventual acceptance as the preferred form of ESS worldwide [6].

There are several studies focusing on optimizing the integration of RE and ESS and our surveys reveal that most of them are wind energy centric [22]–[34] and only a handful are on solar energy [35]–[37]. Among these studies, [29], [30], [33], [35], [37] modelled the integration based on the reliability of generation and transmission network and, [23]–[25], [27], [34], [36] expanded the work by adding the economic factor, which critically influence the overall socio-economic benefit of the model. Different algorithms such as harmony search (HS), simulated annealing (SA) and Tabu search have been used to solve the above optimizations due to the conflicting objectives of minimizing RE's operation cost and load curtailment [38]–[41]. The Monte Carlo simulation method has also been used to simulate the stochastic behaviour of RE sources and the large combinations of generation system states [23], [26], [37]. But due to its long computational time, the analytical technique has also been used although the calculations are less accurate [24], [25], [33]. Nonetheless, all the studies mentioned above have collectively demonstrated the technological advantage of the BESS over other technologies in enhancing the penetration of RE. In summary, these studies focus on optimizing the capacity-cost ratio [23], [30], [37], [42], [43], installation site [22], [32] and the usage-lifetime cycle [27] of the BESS that is the most beneficial for utilities and RE operators.

Notwithstanding the cited work, several common drawbacks are identified. First, they were mostly focused on optimizing various aspects of BESS only. As a result, the optimum level of the RE penetration were neglected and, hence violating energy blueprints of most countries which seek to determine the optimum percentage of RE within their generation systems; such analyses neglect the relationship between the optimum levels of RE and BESS which can significantly alter their installation and operational decisions. Secondly, in the cases where the RE were optimized, none of them holistically considered reliability, economy, societal and environmental impacts in their optimizations. Due to this, the results presented are most of the time overly optimistic and this can increase the operation risk in practical applications. Thirdly, the lack of accurate modelling of the RE sources, in the case of this paper the solar irradiation and wind speed, inhibits their accurate simulations and eventually leading to optimizations that are bias.

In view of the highlighted shortcomings, this paper proposes a two-step optimization technique based on genetic algorithm to optimize the penetration of RE and installation of BESS as a way to fill the first identified gap above. Given that photovoltaic (PV) and wind farms are currently the two most popular types of RE evidenced by their wide coverage in the cited literatures above, the proposed formulation considered only the solar and wind farms. Secondly, the proposed optimization considers the costs of RE-integrated generation system and BESS, as well as their operation risk in such a way that these aspects are embedded into cost functions of the optimization. As suggested in [44], we carefully formulated the cost functions and link them through Pareto fronts ranking in order to obtain the optimum design of generation system. Throughout the optimization, real constraints of the PV, wind farms and the BESS are also considered to ensure a sufficient degree of practicality in the proposed methodology. As per any reliability studies, the reliability aspect of the proposed framework is performed using the sequential Monte Carlo simulation (SMCS) [45] and the IEEE 24-bus Reliability Test System (RTS) is chosen as the studied system [46]. With this, the second identified drawback is addressed by our proposed optimization. Thirdly, the proposed optimization is also accompanied by the state-of-art modelling of the solar radiation and wind speed to ensure that our optimization is not influenced by the simulation errors of these weather parameters.

The remaining paper is organised as follows. Section II outlines the proposed optimization of RE (PV and wind) and BESS capacity, as well as, the modelling of solar radiation, wind speed and BESS. Section III presents results and discussions of the performed optimization, and finally, Section V concludes the paper.

## II. METHODOLOGY

A two-step optimization model is proposed such that the first part optimizes the penetration of RE and second part optimizes BESS capacity. The two-step approach is preferred over the single framework to reduce computational [47]. In this first part, important elements affecting reliability, economic and societal factors are embedded as multiple cost functions, which are all derived from actual industry standards. The costs are conflicting with each other as no cost terms can be reduced without sacrificing other costs. For example, the load curtailment cost can only be reliably reduced by installing more CG units. However, this leads to the undesirable effect of reducing the penetration of RE and subsequently raises the environmental costs. On the other hand, although increasing the penetration of RE can reduce the environmental cost, the intermittency of the RE sources can potentially cause more demand losses and lead to the higher load curtailment cost. In view of the highlighted conflicts, the presented costs above should be considered separately rather than being lumped as a single cost; finding the optimal trade-offs among all the costs becomes a multi-objective optimization problem that this paper intends to solve. In the second part, the proposed methodology optimizes the installation of the BESS based on the optimal level of RE identified in the first part. Therefore, the objective functions from the first part are reconsidered and further

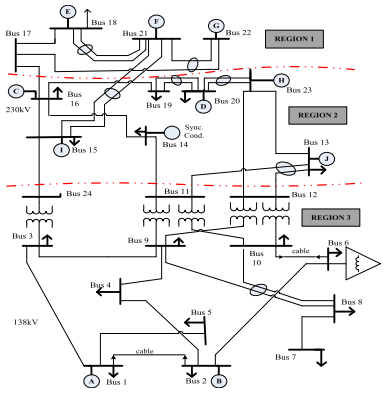


**FIGURE 1.** Modified IEEE 24-bus RTS.

refined in the second part. The modelling details are presented next.

### A. RELIABILITY TEST SYSTEM

The IEEE 24-bus RTS [46] is used in this paper. It consists of 32 generating units, 10 generator buses and 17 load busses. The total generating capacity and peak load are 3405 MW and 2850 MW, respectively. The RTS used in this paper is slightly modified as shown in Fig. 1. It shows that the RTS is divided into three regions, notated as Region 1, 2 and 3. The distance between these regions are about 50 km apart. The locations of the generators are notated as A, B, C until J and they are all candidates to host wind and solar farms. Due to this, weather data from 10 different locations are required for the modelling of the wind and solar generation systems. Following this, 15-year of historical weather data with 1-hour resolution, ranging from 2000 to 2014, were sampled from 10 different locations in Thailand [48].

One of the important factors of wind speeds and solar radiations is their stochastic properties and modelling it is paramount to ensure realistic simulations of their data [49]. It was found in [50] that wind speed is most suitable to be modelled using the Auto-regressive Moving-Average (ARMA) model (see section II.B ) due to its ability to capture time propagation pattern of wind and, it is also able to avoid biasing by not enforcing any probability distributions onto the wind data. As such, the ARMA model is used in this paper. As for the modelling of the solar radiation, it has been shown that the proposed model in our previously published paper (see section II.B) [51] is more robust than existing models and it is also used in this paper.

In addition to the identified models above, the correlation of weather data is also considered during the simulation of the weather data. The reason is the weather data from locations that are closer to each other display stronger level of correlation than with locations that are further apart. By incorporating this feature, the underlying correlations among the historical data are retained, leading to a more accurate simulation of the weather data. In this paper, the correlation is

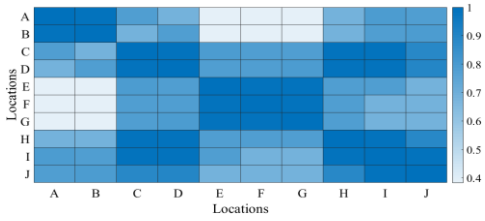


**FIGURE 2.** Correlations among locations.

defined as the following [52]:

$$\rho_{x,y} = \frac{cov(x, y)}{\sigma_x \sigma_y} \tag{1}$$

where $\rho_{x,y}$ is the correlations between vector $x$ and $y$; $\text{cov}(x, y)$ is the covariance between the two vectors and $\sigma$ is the standard deviation of each vector, i.e. the weather data.

A heat map is presented in Fig. 2 to illustrate the correlations of the sampled wind and solar data. The figure shows that the correlations of the weather data from the same locations are stronger than with other locations. For example, the weather data at location A and B have strong correlation value of about 0.90 as they are from within the same region. However, the value reduces to about 0.3 when the data at location B and G are compared. The reason is location G is in region 1 that is much further away from region 3. The observation shows that the differences of correlations among the weather data from different regions and locations are significant and should therefore be taken into account during their simulations. In the next section, the modelling of the solar radiation and wind speed, as well as, the incorporation of their correlation features, are elucidated.

### B. SOLAR AND WIND ENERGY MODEL

#### 1) SOLAR ENERGY CONVERSION SYSTEM

The solar radiation model proposed in our published paper [51] is used in this study. Results have shown that it is able to simulate solar data that is non-stationary, time dependent and adhere to local geographical conditions, which are all important features of the solar radiation. Also shown is that the proposed solar radiation model is more precise and robust than existing popular models, demonstrated by common statistical tests such as the F-test, diurnal distribution test, partial auto-correlation function (PACF) test, as well as mean and standard deviation test that were conducted in the paper. The followings are the brief descriptions of our solar radiation model:

First, consider a $\boldsymbol{Y}$ matrix that contains all the sampled historical solar radiation data which has the following form:

$$Y = [\boldsymbol{M}_1, \boldsymbol{M}_2, \ldots, \boldsymbol{M}_\alpha | \, \alpha = 12] \tag{2}$$

where $\alpha$ is the number of months; $\boldsymbol{M}$ the sub-matrix that groups all the solar radiation data from the same month of the entire sampled solar radiation data. The row and column of the sub-matrix are the hour and day of the solar radiation.

Then, the following steps are performed to model and simulated the solar radiation data.

Step 1: the PACF of every $\boldsymbol{M}$ is determined to identify the number of significant lags.

Step 2: every row of $\boldsymbol{M}$ is clustered using the k-means clustering algorithm, whereby the algorithm will determine the number of necessary cluster. A new matrix $\boldsymbol{M}'$ is derived from $\boldsymbol{M}$ by replacing the existing solar radiation values with their respective cluster numbers. The mean and standard deviation of each row is determined and kept for later usage in Step 5. This essentially indicates that the row values are normally distributed.

Step 3: At each row of $\boldsymbol{M}'$, all the unique combinations, $\boldsymbol{U}$, of previous row values up until the current row are identified and the probabilities, $\boldsymbol{P}$, of all the unique combinations are determined.

Step 4: The obtained matrices $\boldsymbol{U}$ and $\boldsymbol{P}$ are used to guide the simulation of new $\boldsymbol{M}'$, notated by the matrix $\boldsymbol{G}$. Notice that due to the lagging factor determined earlier in Step 1, the simulation of $\boldsymbol{G}$ requires its first few rows, determined by the number of lags, to be initialized with 1, i.e. same cluster, as initial solar radiations from zero hour are always 0.

Step 5: The cluster matrix $\boldsymbol{G}$ is randomly converted into the actual solar radiation. In order to consider the underlying correlations of the solar radiation data amongst the different locations, all the normal distributions at each row of all the locations are combined into the multivariate form such as the following:

$$f(x) = \frac{exp\left\{-\frac{1}{2}(x-\mu)^{\mathrm{T}}\Sigma^{-1}(x-\mu)\right\}}{(2\pi)^{p/2}|\Sigma|^{1/2}} \tag{3}$$

where $p$ is the number of normal distribution; $\mu$ is the mean vector of all the normal distributions; $x$ is the correlated random number vector which has the same number of element as $p$; $\Sigma$ is the covariance matrix of all the normal distributions. Due to the correlation specified in the covariance matrix, all the random number drawn for each normal distribution are correlated in the same manner.

The above steps are applied at every location to obtain their simulated solar radiation data, which is then used to determine the potential solar power production at respective locations. The output power of a PV farm, $P_s(W)$, is calculated as the following [53]:

$$P_S = N_p \times FF \times V_i \times I_i \tag{4}$$

such that,

$$I_i = G_i\left[I_{sc} + K_{sc}(T_c - T_{std})\right] \tag{4a}$$

$$V_i = V_{oc} - K_{oc}T_c \tag{4b}$$

$$T_c = T_i + G_i\left(\frac{T_{nom} - 20}{0.8}\right) \tag{4c}$$

where, in (4), $N_p$ is the number of PV panels; $FF$ is the fill-factor that has been specified by PV panel manufacturer and its value is 0.705 [54]; $V_i$ and $I_i$ are the voltage and current of the PV panel at hour $i$, respectively; in (4a), $G_i(W/m^2)$ is the solar radiation simulated by our model above; $T_c$ (°C) is the cell temperature; $I_{sc}$, $K_{sc}$ and $T_{std}$ are the short-circuit current, short-circuit-current temperature and standard temperature constants set as $5.32A$, $1.22mV/°C$ and 25°C, respectively [54]; in (4b), $V_{oc}$ and $K_{oc}$ are the open-circuit voltage and open-circuit-voltage temperature constants set as $21.98V$ and $14.40\ mV/°C$ [54]; in (4c), $T_i$(°C) is the ambient temperature; $T_{nom}$ is the nominal temperature set as 43°C [54].

### 2) WIND ENERGY CONVERSION SYSTEM

The wind speed data is modelled using the ARMA model (see (5)) as it produces high-order auto-correlation and it is suitable for the modelling of wind speed.

$$y_t = \sum_{i=1}^{n}\phi_i y_{t-i} + \alpha_t - \sum_{j=1}^{m}\theta_j\alpha_{t-j} \tag{5}$$

where $y_t$ is the simulated wind speed at time $t$; $\phi_i$ and $\theta_j$ are the auto-regressive (AR) and moving-average (MA) parameters, respectively; $\alpha_t$ is a normally and independently distributed (NID) random white noise with zero mean and standard deviation of $\sigma$ (i.e. $\alpha_t \in NID(0, \sigma)$);

From (5), it is shown that $y_t$ is dependent on its previously simulated values, $(y_{t-i}|\, i = 1, 2, \ldots, n)$, and random white noises, $\left(\alpha_{t-j}\middle|\, j = 1, 2, \ldots, m\right)$. The order pair of the stationary ARMA model $(n, m)$, is reduced to $(n, n-1)$ [50], [55]. In order to consider the underlying correlation of the wind speed data during its simulation, the same process used for generating correlated random numbers in the solar radiation modelling is repeated here. In this case, the normal distributions of white noise at all the locations are combined into the multivariate form as in (3).

Based on the simulated wind speed values, the potential wind power output at each location is obtained as in (6) [56] which is also illustrated in Fig. 3.

$$P_w = \begin{cases} 0, & 0 \le V_w < V_{ci} \\ \left(A + BV_w + CV_w^2\right)P_r, & V_{ci} \le V_w < V_r \\ P_r, & V_r \le V_w < V_{co} \\ 0, & V_w \ge V_{co} \end{cases} \tag{6}$$

where $P_w$ is the wind farm power output; $V_w$ is the simulated wind speed; $V_{ci}$, $V_r$ and $V_{co}$ are the cut-in, rated and cut-out wind speeds, respectively; $P_r$ is the rated power of the wind farm. Equation (6) shows that wind farms only generate power when the wind speed is between cut-in and cut-out speeds. For safety reasons, wind farms stop generating power when the wind speed is above the cut-out speed. The constants A, B and C are as the followings [57]:

$$A = \frac{1}{(V_{ci}-V_r)^2}\left[V_{ci}(V_{ci}+V_r) - 4(V_{ci}V_r)\left(\frac{V_{ci}+V_r}{2V_r}\right)^3\right]$$

$$B = \frac{1}{(V_{ci}-V_r)^2}\left[4(V_{ci}V_r)\left(\frac{V_{ci}+V_r}{2V_r}\right)^3 - (3V_{ci}+V_r)\right]$$

$$C = \frac{1}{(V_{ci}-V_r)^2}\left[2 - 4\left(\frac{V_{ci}+V_r}{2V_r}\right)^3\right] \tag{7}$$

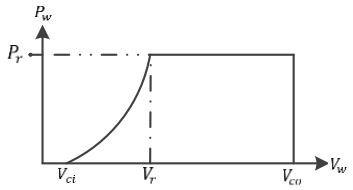


**FIGURE 3.** WTG Output Power Model.

### C. BESS MODEL

BESS alongside RE units can reduce power supply fluctuations caused by the intermittency of the RE sources. As a result, the BESS is also able to mitigate hefty penalty charges for undelivered power supplies that have been contracted earlier by RE units. Moreover, it also cushions the reliability and economic risks that arise from the errors of the weather models that cannot be avoided. The modelling details of the BESS is described here. First, consider the following:

$$SG^i_{RE} = TG^i_{RE} - X\% \times L_i \tag{8a}$$
$$SG^i_{CG} = TG^i_{CG} - (1 - X\%) \times L_i \tag{8b}$$

where $SG^i_{RE}$ and $SG^i_{CG}$ are the total surplus capacity of the RE and CG units; $TG^i_{RE}$ and $TG^i_{CG}$ are the total capacity of the RE and CG units; $L_i$ is the total load level; the notation $i$ refers to the state at a particular hour; $X\%$ is the portion of the load level that is committed to be supplied by the RE units. Notice that when the load level is higher than the capacity of the generators, the surplus capacity, $SG^i_{RE}$ and $SG^i_{CG}$, can become negative.

Then, the state-of-charge (SOC) of the BESS at each hour is determined according to the operation policy of the BESS. In the first policy, the BESS is used whenever the total generation capacity is unable to meet the load demand. In other words, both the RE and CG units are used to support each other despite the load commitment level determined earlier. This policy is as the following:

$$SOC_{i+1} = \begin{cases} SOC_i + SG^i_{RE} & SG^i_{RE} \geq 0 \quad SG^i_{CG} \geq 0 \\ SOC_i + SG^i_{RE} & SG^i_{RE} \geq 0 \quad TSG^i \geq 0 \\ SOC_i & SG^i_{RE} < 0 \quad TSG^i \geq 0 \\ SOC_i + TSG^i & SG^i_{RE} < 0 \quad TSG^i < 0 \end{cases} \tag{9}$$

where $TSG^i = SG^i_{RE} + SG^i_{CG}$ is the total surplus generation. The first line of (9) indicates when there are surplus capacities of RE and CG units. As a result, the additional generated RE power is stored in the BESS. The second line of (9) describes the condition when the total surplus generation is enough to support the entire load demand and there is still surplus RE power and the BESS is therefore charged with the RE power; this indicates that the CG units are only slightly not enough to meet the load demand and the power gap can be filled by the relatively small capacity of the RE units. The third line is similar to the second one except there is no more surplus RE power and, as a result, the SOC of the BESS remains unchanged; this is the condition when the surplus of the CG units is sufficient to meet the load demand dedicated to the RE units. However, the RE units are incapable to meet its entire dedicated load demand. The final line is when the capacity of the RE units is low and this coincides with multiple CG unit failures. As this results in no surplus of total generation, the BESS has to be discharged to support the load demand instead.

In the second policy, the BESS is dedicated to support the RE units only. In contrast to the first policy, there is no collaboration between the RE and CG units in the second policy and it is as the following:

$$SOC_{i+1} = \begin{cases} SOC_i + SG^i_{RE}, & SG^i_{RE} \geq 0 \& SG^i_{CG} \geq 0 \\ SOC_i + SG^i_{RE}, & SG^i_{RE} < 0 \end{cases} \tag{10}$$

the first line of (10) shows both the RE and CGU units are in the surplus. Due to the surplus in the RE units alone, the BESS is charged with the additional RE power for later usage. The second line indicates that as long as there is no surplus RE power, the BESS is discharged to support the load demand.

In the third policy, the BESS is used to support both the RE and CG units, but its priority is given to the RE units. Similarly to the second policy, the CG and RE units are not used to support each other here. The third policy is as the following:

$$SOC_{i+1} = \begin{cases} SOC_i + SG^i_{RE}, & SG^i_{RE} \geq 0 \& SG^i_{CG} \geq 0 \\ SOC_i + SG^i_{RE}, & SG^i_{RE} < 0 \\ SOC_i + SG^i_{CG}, & SG^i_{RE} \geq 0 \& SG^i_{CG} < 0 \end{cases} \tag{11}$$

the first line of (11) shows that when the surpluses of both the CG and RE units are more than zero, the additional RE is stored in the BESS for later usage. The surplus of the CG units is not considered as their power generation can be controlled. The second line of (11) indicates that as long as there are inadequacies of RE, the BESS is discharged to support the power supply. The third line shows that the BESS is also discharged to support the power supply of the CG units when their capacity is inadequate to meet load demands.

The BESS is also constrained by linear charging/discharging rate, as in the following:

$$C_R = (SOC_{max} - SOC_{min}) \,/\, T \tag{12}$$

where $C_R$ is the maximum charging/discharging rate of the BESS; $\text{SOC}_{max}$ is the maximum rated capacity of the BESS taken as a percentage of the total installed capacity of the RE units; $\text{SOC}_{min}$ is the minimum capacity of the BESS set at 20% of $\text{SOC}_{max}$ to maintain the longevity of the BESS; $T$ is charging/discharging period. From (12), the inequality $P^i_{chg} \leq C_R$ holds such that $P^i_{chg}$ is the charging/discharging power of the BESS at any time.

### D. MULTI-OBJECTIVE FUNCTION COST MODEL

#### 1) PART 1: OPTIMIZING RE LEVEL

The first part of the proposed optimization algorithm determines the optimal penetration level of RE based on three objective functions.

The first objective is the social cost, as the following:

$$min\,(f_1) = C_{EENS} + C_{Env} \tag{13}$$

Such that,

$$C_{EENS} = \sum_{t=1}^{T} \lambda_{ENS} ENS_t \tag{14}$$

$$C_{Env} = C_p^{env} \left( \sum_{i=\Omega_{oil}} \alpha_i X_i \mu_i + \sum_{j=\Omega_{gas}} \beta_j X_j \mu_j + \sum_{k=\Omega_{coal}} \gamma_k X_k \mu_k \right) \tag{15}$$

where in (14), $C_{EENS}$ is the load curtailment cost; $\lambda_{ENS}$ is the multiplication factor for every unit of unsupplied energy demanded and is considered as \$5270/MWh [58]; $ENS_t$ is the amount of energy-not-supplied at hour $t$ in MWh; in (15), $C_{Env}$ is the environmental cost; $\Omega_{oil}$, $\Omega_{gas}$ and $\Omega_{coal}$ are the set of turbine generators fired by oil, gas and coal, respectively; $\alpha$, $\beta$ and $\gamma$ are the binary decision for whether the respective types of generators are included in the power system; $X$ is the installed capacity of the generators in MW; $\mu$ is the amount of carbon emitted by each type of generator with respect to their capacity, which is set as 1362.5 tonnes/MWh for oil-fired generators, 1638 tonnes/MWh for gas-fired generators and 1840 tonnes/MWh for coal-fired generators [59]; $C_p^{env}$ is the environment pollution tax considered as \$5/tonne [60].

The second objective function is the utility system cost, as the following:

$$\begin{aligned} min\,(f_2) = & \sum_{i=\Omega_{CT}} \alpha_i X_i \left( C_i^{cap} + C_i^M \right) \\ & + \sum_{j=\Omega_{stm}} \beta_j X_j \left( C_j^{cap} + C_j^M \right) \\ & + \sum_{k=\Omega_{coal}} \gamma_k X_k \left( C_k^{cap} + C_k^M \right) \\ & + \sum_{l=\Omega_{nuc}} \varepsilon_l X_l (C_l^{cap} + C_l^M) \end{aligned} \tag{16}$$

where $\Omega_{nuc}$ is the set of all nuclear generators; $\varepsilon$ is the binary decision for whether the nuclear generator is included in the system; Notice that the nuclear generators are not included in (15) as they have no carbon emission; $C^{cap}$ and $C^M$ are the capital and maintenance costs of the generators in \$/MWh. The capital and maintenance costs are the same in the oil-fired and gas-fired generators, which are \$409/MWh and \$10.22/MWh, respectively. The capital and maintenance costs of coal-fired generators are \$1154/MWh and \$24.52/MWh, respectively. Nuclear-based generators are the most expensive with capital and maintenance cost of \$2117/MWh and \$58.48/MWh, respectively [61].

The third objective function is the independent RE operating cost, as the following:

$$min\,(f_3) = \sum_{m=\Omega_{RE}} \kappa_m X_m \left( C_m^{cap} + C_m^M \right) \tag{17}$$

where $\Omega_{RE}$ is the set of all installed RE units, which can either be PV or wind farms; $\kappa$ is the binary decision for whether the RE unit is installed to replace one of the 10 CG units in the RTS; the investment cost of both PV and wind farms are \$1267/kWh and \$1178/kWh, respectively [62].

#### 2) PART 2: OPTIMISING BESS SIZE

Adding BESS units will impose additional utility system costs and directly affecting the second objective function in (16). Therefore, it is refined and optimized as the following:

$$min\left(f_2^{new}\right) = f_2 + C_{BESS} \tag{18}$$

such that,

$$C_{BESS} = \phi X_{RE} \left( C_{BESS}^{cap} + C_{BESS}^M \right) \tag{19}$$

where $f_2$ is the optimized objective function values inherited from (16); $\phi$ is the percentage value used to control the installed capacity of the BESS; $X_{RE}$ is the optimized capacity of the RE units in the first part; $C_{BESS}^{cap}$ and $C_{BESS}^M$ are the capital and maintenance cost of BESS in \$/MWh, respectively. The reported capital cost is \$357/MWh, whereas the maintenance cost is set as 2.5% of the capital cost, which is \$8.925/MWh [63], [64].

The first objective function in (13) is also updated as the presence of the BESS changes the power-demand relationship. The third objective function in (17) is unaffected as the penetration of RE units has been determined in the first part. Hence in this second part, the size of the BESS is optimized based only on (13) and (18).

### E. MULTI-OBJECTIVE GENETIC ALGORITHM

The objective functions defined earlier in section II.D are conflicting with each other. Due to this, there have to be compromises in the optimization of all the objective functions and, as a result, this produces a set of non-dominated optimality known as Pareto solutions [65]. In order to qualify as a Pareto solution, none of the objective functions can be improved without degrading the other functions, and a set of Pareto solutions found is known as the Pareto front. This paper employs the non-dominated-sorting genetic algorithm (NSGA) to solve the optimization problem. Upon obtaining the Pareto front, the NSGA is capable of sorting the members of the front according to their non-dominancy levels. The following is the step-by-step process of the NSGA:

***Step 1*:** randomly initialize the first set of candidate solution, also known as individual, to fill the first generation of population. In the first part of the optimization, the first population has only 32 random binary numbers as there are

32 potential CG units in the RTS that can potentially be replaced with RE units.

***Step 2*:** replace the respective CG units with RE units according to the population. Then, use the sequential Monte Carlo simulation (SMCS) technique to perform generation system reliability analysis of the RTS. The purpose of the analysis is to obtain the expected value of ENS (EENS) and carbon emission level in (14) and (15), respectively, which will then produce the expected cost of the first objective function in (13). The second and third objective functions ((16) and (17)) are determined only by the number and not by the power output of CG and RE units and are therefore not affected by the SMCS. The following is description of the SMCS process:

*Step 2.1*: initialize all CG and RE units in the up-state. Determine the time-to-failure (TTF) and time-to-repair (TTR) of all the generating units according to $-1/\omega \ln U$, such that $\omega$ is either the failure or repair rates, collectively known as the reliability data, of the generators. $U$ is the uniform random number. The reliability data of CG units are given in the RTS. The considered failure and repair rates of wind farms are 1.51/year and 125.14/year, respectively, and of the PV farms are 4.56/year and 109.50/year hours, respectively [66], [67].

*Step 2.2*: the up-down cycle of all the generators (CG and RE units) are simulated for every hour based on their respective TTF and TTR obtained in *Step 2.1*. The hourly chronological load level given by the RTS is also identified. Only the load level on the second day of the 51$^{st}$ week is used as this day represents the peak load level throughout the entire year of the RTS. CG units that are in the up-state is considered to have the full rated capacity. The hourly solar radiation and wind speed values are simulated based on the weather models in section II.B, which are then used to determine the capacity of the RE units that are in the up-state.

*Step 2.3*: the total load and generation mismatch is calculated to determine the load curtailment cost, $C_{EENS}$, and environmental cost, $C_{Env}$, which are both used to update the first objective function in (13). The expected-energy-not-supplied (EENS) index is also updated.

*Step 2.4*: *Step 2.2* and *Step 2.3* are repeated until the SMCS is converged, which is when the coefficient variation of the EENS drops below 5%

***Step 3*:** the objective function values in (13), (16) and (17) are determined based on the output of SMCS.

***Step 4*:** sort the candidate solutions into the Pareto front based on their levels of non-dominancy. The next generation of candidate solutions, also known as children, is produced according to the classical GA operators, i.e., mutation, crossover and elitism. Each population size is limited to 200 individuals.

***Step 5*:** the function tolerance of the solutions are calculated to determining the stopping criteria of the NSGA, which is defined as when the average relative change in the best fitness function (also known as objective) values is less than $10^{-4}$ over 100 generations.

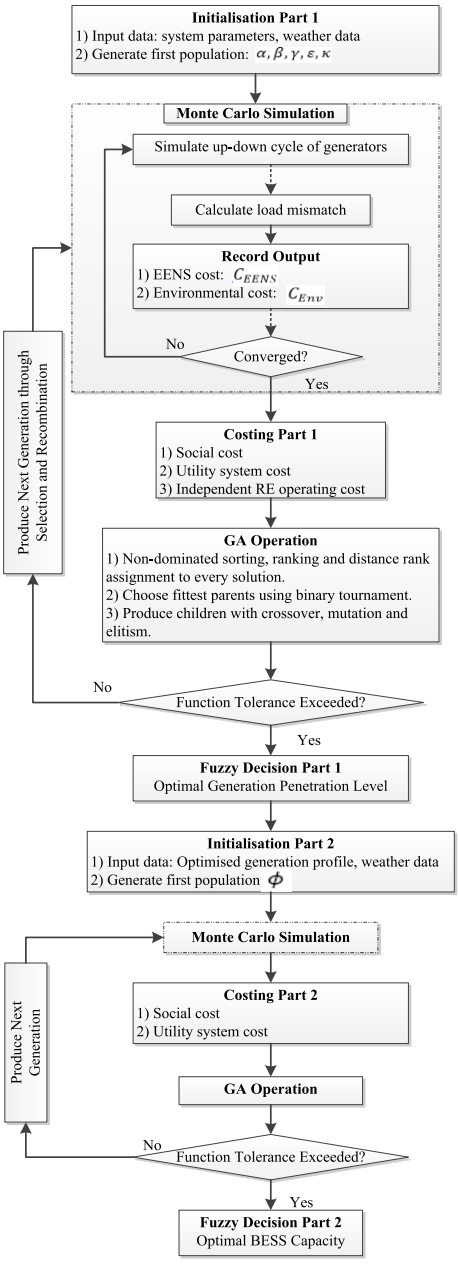


**FIGURE 4.** Flowchart of the proposed NSGA.

***Step 6*:** if the function tolerance is not met, the next generation of population is produced based on the GA selection and recombination operation and the process will restart at ***Step 2***. Otherwise, the Pareto front of CG and RE unit mixtures has been adequately obtained and one solution in the Pareto front is selected.

Due to multiple equally optimum solutions in the Pareto front, a solution is decided based on the fuzzy decision making process [68]. The fuzzy method works by assigning membership function values to each objective function and then ranks the Pareto solutions. The membership function (MF) values range from 0 to 1, which denote total compatibility and incompatibility between the objective and preference.

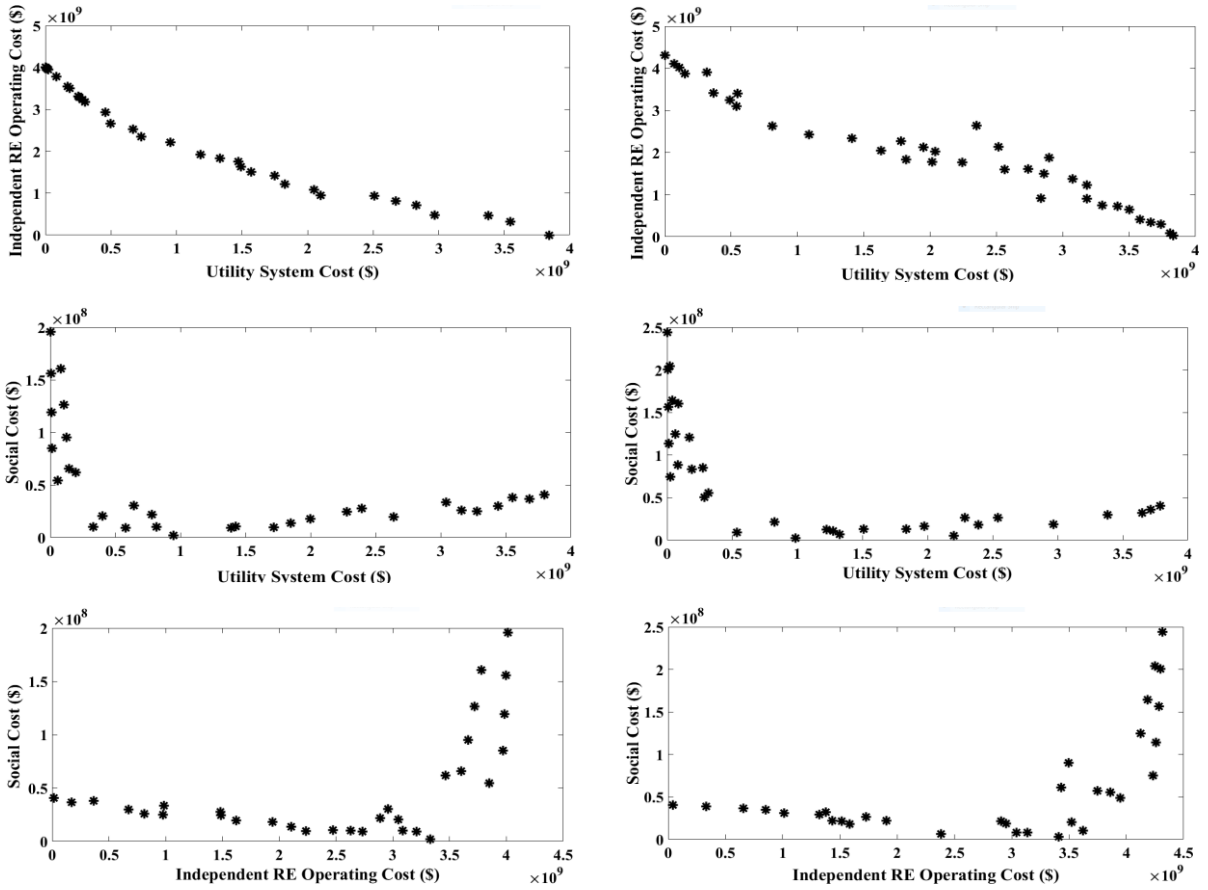


**FIGURE 5.** Non-dominated solutions and trade-offs for the penetration of PV ((a) – (c)) and wind ((d) – (f)) farms. c)).

The assignment of the MF value is as such:

$$\psi_{f_i}(x) = \begin{cases} 0, & f_i(X) \geq f_i^{max} \\ \dfrac{f_i^{max} - f_i(X)}{f_i^{max} - f_i^{min}}, & f_i^{min} < f_i(X) < f_i^{max} \\ 1, & f_i(X) \leq f_i^{min} \end{cases} \quad (20)$$

where $\psi_{f_i}(X)$ denotes the membership function value of a particular solution $X$ in the objective function $f_i$; $f_i^{max}$ and $f_i^{min}$ are the maximum and minimum values of the objective function, respectively.

Then, the final solution is selected based on the preference setting for each objective function, denoted by $\psi_{f_i}$, such as the following:

$$\min_{X \in \Omega_p} (K_X) = \sum_{i \in \Omega_f} \left( \left| \psi_{f_i} - \psi_{f_i}(X) \right|^n \right), \quad 1 \leq n < \infty \quad (21)$$

where $\Omega_P$ is the set of Pareto solution; $\Omega_f$ is the set of objective functions; (21) shows that the Pareto solution that yields the minimum sum of difference between preference and membership function values is the preferred solution; $n$ is any large integer number but selecting a number that is too large will reduce the sensitivity of the selection process.

***Step 7:*** in the second part of the optimization, the selected optimum mixture of CG and RE units is retained. Then, randomly initialize the first population, which is a random percentage value used to determine the size of the BESS. SMCS is executed to determine (18) and update (13). The GA operation rules used to produce the next generation and to determine the stopping criteria are the same as previously mentioned. The fuzzy selection process in (20) and (21) is also applicable here to select the optimum BESS size from among its Pareto front. The simulation process is enhanced by graphics processing unit (GPU) accelerated computing to fasten the computational time [64].

The overview of the described NSGA process is illustrated in Fig. 4.

## III. RESULTS AND DISCUSSION

### A. OPTIMIZATION OF RE PENETRATION LEVEL

The proposed NSGA was executed separately when determining the optimum penetration level of PV and wind farms and the obtained Pareto fronts are shown in Fig. 5. Fig. 5 (a) – (c) show that integrating PV farms produces at most \$200M, \$3800M and \$4100M in social cost, utility system cost and RE cost, respectively. In contrast, these values are 250M\$, 3800M\$ and 4400M\$ as shown in Fig. 5 (d) – (f) when PV farms are replaced with wind farms. Notice that the social and RE costs are higher when wind farms are considered. The higher social cost indicates

**TABLE 1. Final optimal solutions of PV and Wind farms.**

| Measurement | PV | Wind |
|---|---|---|
| Penetration level (%) | 48.34 | 40.44 |
| CG units replaced | 2,3,4,7,10,11, 13,19,21,24,25, 30,32 | 2,4,6,7,9,13,15, 17,18,19,20,22,24 ,27,28,29,31,32 |
| Social cost (M$) | 36.01 | 38.52 |
| Utility system cost (M$) | 1996.50 | 2286.90 |
| RE cost (M$) | 1939.00 | 1744.70 |

that wind fluctuates more than the solar radiation over the same period of time, leading to greater intermittency in wind farm operations, and causes higher probability of load loss and social cost. Moreover, our simulation also shows that the average PV power output from all the locations is about 4.29 MW/hour, which is much higher than the wind power output of about 1.07 MW/hour only. As for the higher RE cost, it is due to the higher capital and maintenance costs of wind farms as compared to PV farms.

The results in Fig 5 (a) – (f) also show that the relationships among the objective functions are similar in both the PV and wind farms. For example, both Fig. 5 (a) and (d) show that the utility system cost increases as the RE cost reduces and vice versa. This makes sense as RE and CG units are always competing with each other to fill the generation profile during the optimization. Both Fig 5 (b) and (e) show that the utility system cost increases as the social cost reduces and vice versa. Higher utility system cost indicates that more CG units are used instead of RE units and due to their stable power production the load curtailment cost reduces much faster and more significantly than the increment of environmental cost, which the summation of both causes the social cost to reduce. In other words, the penalty of the environmental cost should be increased in the future if the effect of carbon emissions is to have more influence on the penetration of the RE systems. Finally, both Fig. 5 (c) and (f) show that the social and RE costs increase together. The reason is a higher RE cost indicates a greater penetration of RE units and, due to their intermittency the reliability of the power system reduces without the support of the BESS, leading to the increment of social cost.

Among the Pareto solutions of PV and wind farm penetration cases, a solution is separately selected for both based on the described fuzzy decision-making process. The preferences set for objective functions in (13), (16) and (17) are $\psi_{f_1} = 0.8$, $\psi_{f_2} = 0.5$ and $\psi_{f_3} = 0.5$, respectively, and the results are shown in Table 1. These sets of selected optimal solutions are retained in the next section when optimizing the size of the BESSs.

### B. OPTIMISATION OF BESS SIZE

In this section, the BESS is incorporated into the RTS and its size is optimized. Recall that the objective functions used in this section are (13) and (18) only, which are the social and utility system costs. Based on the selected optimum solutions of PV and wind farms integration in section III.A, first BESS policy and 4-hour battery charging/discharging period, Pareto solutions of the installed BESS size in these two cases are obtained and plotted in Fig. 6 (a) and (b), respectively. The results in the two figures show that the social cost reduces as the utility system cost increases. An increased in the utility system cost signifies that a larger capacity of the BESS is installed and hence, more power is available to be discharged for meeting load demand, subsequently driving down the social cost.

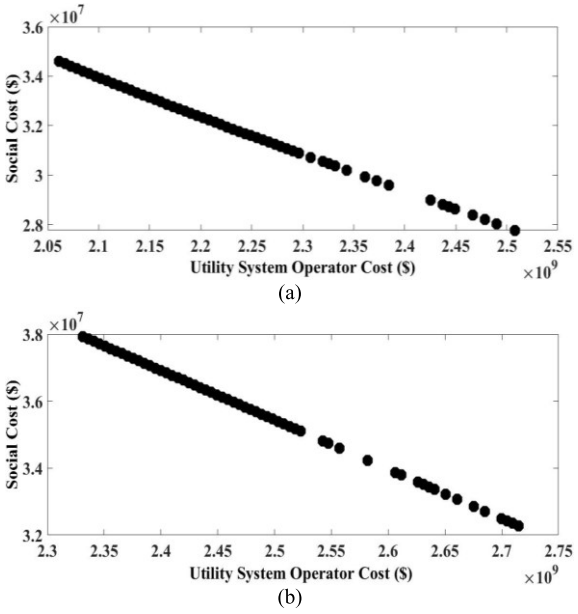


**FIGURE 6. Non-dominated solutions and trade-offs for the installation of the BESS in the PV ((a)) and wind ((b)) farms integrated RTS.**

The fuzzy decision-making process described in (20) and (21) is also applied to the Pareto front here and the selected optimum solutions are shown in Table 2. The results in the table show that the optimum BESS capacity in both the PV and wind farms penetration cases are about the same, 59% and 60%, respectively. Also shown is that the social costs in both cases have reduced, as compared with Table 1, by about 16.1% and 11.1% in the PV and wind cases, respectively. However, the utility system costs of the two cases have respectively increased by about 17.4% and 12.9%. The RE costs are not reported in Table 2 as their values in Table 1 remain unchanged. The higher utility system costs point out that about 970 MW and 871 MW of BESS are installed in the PV and wind cases, respectively.

### C. SENSITIVITY ANALYSES

#### 1) EFFECTS OF PREFERENCE SETTINGS

The effects of the preference settings towards the final selected optimum solutions are investigated and only the PV case is selected to demonstrate the effects. First of all, three sets of preference settings, including the one originally used

**TABLE 2.** Final optimal solutions of PV and Wind farms.

| Measurement | PV | Wind |
|---|---|---|
| Optimum BESS capacity (%) | 59.0 | 60.0 |
| Social cost (M$) | 30.20 | 34.23 |
| Utility system cost (M$) | 2343.20 | 2581.90 |

**TABLE 3.** Selected optimal solutions of various preferences.

| Measurement | $\psi_{f_1} = 0.8$ $\psi_{f_2} = 0.5$ $\psi_{f_3} = 0.5$ | $\psi_{f_1} = 0.5$ $\psi_{f_2} = 0.8$ $\psi_{f_3} = 0.5$ | $\psi_{f_1} = 0.5$ $\psi_{f_2} = 0.5$ $\psi_{f_3} = 0.8$ |
|---|---|---|---|
| Social cost (M$) | 36.91 | 30.35 | 33.54 |
| Utility cost (M$) | 1996.50 | 640.54 | 3041.70 |
| PV cost (M$) | 1939.00 | 2958.00 | 982.45 |
| Penetration (%) | 48.34 | 73.74 | 24.49 |

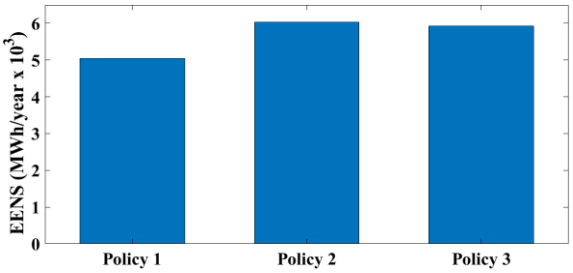


**FIGURE 7.** Reliability effects of various BESS operation policy.

in section III.A, are identified. Table 3 shows the values of these preferences and the optimum decisions selected as a result of the settings.

The first set of solutions is the same as in Table 1. In the first solution, more emphasis is given to the minimisation of the social cost, whereas the utility system and PV costs are equally preferred. Due to this, the social cost is the lowest among the three costs and the utility system and PV costs are about the same. The second set of solution shifts the emphasis to the utility system cost while the remaining costs have equal preferences. As a result, the utility system cost reduces drastically by about 67.9% as compared to the first solution set. In order to enable this, most of the CG units have been replaced with the PV farms and this resulted in about 73.74% of PV penetration, the highest among all the solutions. Finally, in the third set of solution, the minimization of the PV cost is emphasized. This setting resulted in the lowest PV penetration level, registering a reduction of about 49.25% from the second solution set, consequently causing this solution to have the highest utility system cost.

### 2) EFFECTS OF BESS OPERATING POLICY

The optimization so far was performed based on the first policy of BESS. In this section, the effects of the remaining two BESS operation policies toward the EENS of RTS are investigated. The selected solution of the PV penetration level in Table 1 and 4-hour battery charging/discharging period are used to demonstrate this effects and the results, as shown in Fig. 7. The results show that Policy 1 has the lowest EENS, followed by Policy 3 and Policy 2. The reason Policy 1 performs the best is it allows the BESS to support the entire load of the RTS and, at the same time, the PV and CG units are used to support the power capability of each other, leading to a very robust generation system. In contrast, Policy 2 only allows the BESS to be used on the PV farms and this significantly limits the opportunity to support the power-demand gap. Policy 3 is similar to Policy 1 but the BESS in the third policy is mostly used on the PV farms only. As a result, this increases the EENS of Policy 3 by about 17.5% as compared to Policy 1, however it is still lower than Policy 2 by about 1.8%.

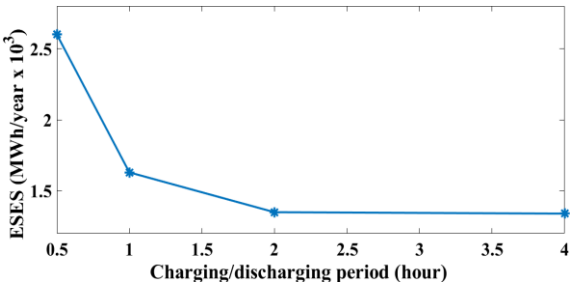


**FIGURE 8.** Effect of charging/discharging period on ESES.

### 3) EFFECT OF CHARGING/DISCHARGING RATES

Based on the selected solution of the PV penetration level in Table 1 and the first BESS operation policy, the reliability effects of the battery charging/discharging rate is studied in this section. The utilized charging/discharging periods are 0.5-, 1-, 2- and 4-hour, respectively. In addition to the EENS, the new expected-surplus-energy-stored (ESES) index such as the following is used to record the expected amount of energy that is saved in the battery:

$$ESE_i = \begin{cases} C_R, & SOC_i \geq C_R \\ SOC_i, & 0 \leq SOC_i < C_R \\ 0, & SOC_i < 0 \end{cases} \tag{22}$$

$$ESES = \frac{1}{N} \sum_{j=1}^{N} \sum_{i=1}^{24} ESE_i \tag{23}$$

where $ESE_i$ is the expected surplus energy at hour $i$ (MWh); $N$ is the number year/simulation;

Fig. 8 and 9 show the effects of charging/discharging rates on ESES and EENS. The results in Fig. 8 show that ESES reduces as the charging/discharging period increases. The reason is the battery with larger period requires longer time to charge/discharge a certain amount of power as compared to the battery with smaller period. This phenomenon is also demonstrated in (12) where it shows the charging/discharging

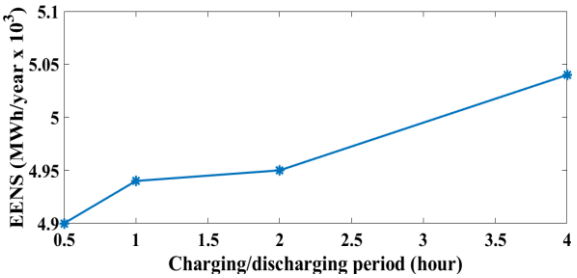


**FIGURE 9.** Effect of charging/discharging period on EENS.

rate is inversely proportional to the charging/discharging period of the battery. On the other hand, the EENS shown in Fig. 9 increases as the charging/discharging period of the battery increases. For the same reason mentioned earlier, larger period leads to longer charging/discharging time, subsequently less additional energy is made available at any time and this causes greater probability of load loss.

## IV. CONCLUSION

A novel two-step procedure for optimal implementation of RE-BESS integrated power system is proposed in this paper. The proposed optimisation covers reliability, operational and environmental aspects of the system, which are further expressed as separate cost functions due to their conflicting objectives. Therefore, the NSGA is used to search for the Pareto fronts that contain all optimal solutions of the objectives. Eventually, a set of the final optimal solutions was determined using the fuzzy decision-making method, which takes into consideration the preferences of decision makers. During the optimization, the time-series behaviour of wind and solar farms is included to ensure a certain level of practicality, in which the correlations among the weather data are also considered. Various operating policies and constraints of the BESS system is considered as well.

Our results show that solar energy is superior to wind in the investigated region. Solar farms produce greater reliability benefit due to less fluctuation of power generated, consequently leading to higher PV penetration level. At the same time, the environmental emission is also reduced with the reduction of CG units. As the capacity of the BESS increases, the social cost is reduced due to more available power to be charged/discharged at any time for matching load demand. The final optimum BESS capacity for both wind and solar are about the same, which are at about 60% of the total RE capacity installed. The sensitivity analysis of the preference settings shows that the proposed algorithm can assist power system planners to decide the best optimum solutions according to their requirements and needs.

## REFERENCES

[1] I. Dincer and M. A. Rosen, "A worldwide perspective on energy, environment and sustainable development," *Int. J. Energy Res.*, vol. 22, no. 15, pp. 1305–1321, 1998.
[2] I. Dincer, "Renewable energy and sustainable development: A crucial review," *Renew. Sustain. Energy Rev.*, vol. 4, no. 2, pp. 157–175, 2000.
[3] R. Billinton, R. N. Allan, and L. Salvaderi, *Applied Reliability Assessment in Electric Power Systems*. New York, NY, USA: IEEE Press, 1991.
[4] H. Abunima, J. Teh, C.-M. Lai, and H. J. Jabir, "A systematic review of reliability studies on composite power systems: A coherent taxonomy motivations, open challenges, recommendations, and new research directions," *Energies*, vol. 11, no. 9, p. 2417, 2018.
[5] M. Shahidehpour, "Investing in expansion: The many issues that cloud transmission planning," *IEEE Power Energy Mag.*, vol. 2, no. 1, pp. 14–18, Jan. 2004.
[6] F. Mohamad, J. Teh, C.-M. Lai, and L.-R. Chen, "Development of energy storage systems for power network reliability: A review," *Energies*, vol. 11, no. 9, p. 2278, 2018.
[7] Bagen and R. Billinton, "Impacts of energy storage on power system reliability performance," in *Proc. Can. Conf. Elect. Comput. Eng.*, May 2005, pp. 494–497.
[8] P. Bohm, "International greenhouse gas emissions trading—With special reference to the kyoto protocol," in *Efficiency and Equity of Climate Change Policy*. Copenhagen, Denmark: Nordic Council of Ministers, 1999.
[9] F. Mohamad and J. Teh, "Impacts of energy storage system on power system reliability: A systematic review," *Energies*, vol. 11, no. 7, p. 1749, Jul. 2018.
[10] J. Teh, C.-M. Lai, N. A. Muhamad, C. A. Ooi, Y.-H. Cheng, M. A. A. M. Zainuri, and M. K. Ishak, "Prospects of using the dynamic thermal rating system for reliable electrical networks: A review," *IEEE Access*, vol. 6, pp. 26765–26778, 2018.
[11] J. Teh, C. A. Ooi, Y. H. Cheng, M. Zainuri, and C. M. Lai, "Composite reliability evaluation of load demand side management and dynamic thermal rating systems," *Energies*, vol. 11, no. 2, p. 466, Feb. 2018.
[12] J. Teh, C. M. Lai, and Y. H. Cheng, "Impact of the real-time thermal loading on the bulk electric system reliability," *IEEE Trans. Rel.*, vol. 66, no. 4, pp. 1110–1119, Dec. 2017.
[13] J. Teh, "Uncertainty analysis of transmission line end-of-life failure model for bulk electric system reliability studies," *IEEE Trans. Rel.*, vol. 67, pp. 1261–1268, 2018.
[14] J. Teh and C.-M. Lai, "Reliability impacts of the dynamic thermal rating system on smart grids considering wireless communications," *IEEE Access*, vol. 7, pp. 41625–41635, 2019.
[15] J. Teh and C.-M. Lai, "Risk-based management of transmission lines enhanced with the dynamic thermal rating system," *IEEE Access*, vol. 7, pp. 76562–76572, 2019.
[16] J. Teh and I. Cotton, "Risk informed design modification of dynamic thermal rating system," *IET Gener., Transmiss. Distrib.*, vol. 9, no. 16, pp. 2697–2704, Dec. 2015.
[17] H. Jabir, J. Teh, D. Ishak, and H. Abunima, "Impacts of demand-side management on electrical power systems: A review," *Energies*, vol. 11, no. 5, p. 1050, Apr. 2018.
[18] H. Jabir, J. Teh, D. Ishak, and H. Abunima, "Impact of demand-side management on the reliability of generation systems," *Energies*, vol. 11, no. 8, p. 2155, Aug. 2018.
[19] J. Teh, "Adequacy assessment of wind integrated generating systems incorporating demand response and battery energy storage system," *Energies*, vol. 11, no. 10, p. 2649, 2018.
[20] M. Farrokhabadi, B. V. Solanki, C. A. Canizares, K. Bhattacharya, S. Koenig, P. S. Sauter, T. Leibfried, and S. Hohmann, "Energy storage in microgrids: Compensating for generation and demand fluctuations while providing ancillary services," *IEEE Power Energy Mag.*, vol. 15, no. 5, pp. 81–91, Sep./Oct. 2017.
[21] J. N. Baker and A. Collinson, "Electrical energy storage at the turn of the Millennium," *Power Eng. J.*, vol. 13, no. 3, pp. 107–112, Jun. 1999.
[22] A. S. A. Awad, T. H. M. El-Fouly, and M. M. A. Salama, "Optimal ESS allocation for load management application," *IEEE Trans. Power Syst.*, vol. 30, no. 1, pp. 327–336, Jan. 2015.
[23] S. Bahramirad, W. Reder, and A. Khodaei, "Reliability-constrained optimal sizing of energy storage system in a microgrid," *IEEE Trans. Smart Grid*, vol. 3, no. 4, pp. 2056–2062, Dec. 2012.
[24] C. Wang, B. Jiao, L. Guo, K. Yuan, and B. Sun, "Optimal planning of stand-alone microgrids incorporating reliability," *J. Mod. Power Syst. Clean Energy*, vol. 2, no. 3, pp. 195–205, 2014.
[25] J. Dong, F. Gao, X. Guan, Q. Zhai, and J. Wu, "Storage-reserve sizing with qualified reliability for connected high renewable penetration micro-grid," *IEEE Trans. Sustain. Energy*, vol. 7, no. 2, pp. 732–743, Apr. 2016.

[26] E. Hajipour, M. Bozorg, and M. Fotuhi-Firuzabad, "Stochastic capacity expansion planning of remote microgrids with wind farms and energy storage," *IEEE Trans. Sustain. Energy*, vol. 6, no. 2, pp. 491–498, Apr. 2015.

[27] K. M. Kamble and H. T. Jadhav, "A wind-battery optimal design algorithm for power generation system," *ARPN J. Eng. Appl. Sci*, vol. 10, no. 8, pp. 3566–3571, 2015.

[28] S. H. Karaki, R. B. Chedid, and R. Ramadan, "Probabilistic production costing of diesel-wind energy conversion systems," *IEEE Trans. Energy Convers.*, vol. 15, no. 3, pp. 284–289, Sep. 2000.

[29] Y. Zhang, S. Zhu, and A. A. Chowdhury, "Reliability modeling and control schemes of composite energy storage and wind generation system with adequate transmission upgrades," *IEEE Trans. Sustain. Energy*, vol. 2, no. 4, pp. 520–526, Oct. 2011.

[30] T.-C. Hung, J. Chong, and K.-Y. Chan, "Reducing uncertainty accumulation in wind-integrated electrical grid," *Energy*, vol. 141, pp. 1072–1083, Dec. 2017.

[31] S. Tabatabaee, S. S. Mortazavi, and T. Niknam, "Stochastic scheduling of local distribution systems considering high penetration of plug-in electric vehicles and renewable energy sources," *Energy*, vol. 121, pp. 480–490, Feb. 2017.

[32] M. Ghofrani, A. Arabali, M. Etezadi-Amoli, and M. S. Fadali, "Energy storage application for performance enhancement of wind integration," *IEEE Trans. Power Syst.*, vol. 28, no. 4, pp. 4803–4811, Nov. 2013.

[33] X. Liu and S. Islam, "Reliability evaluation of a wind-diesel hybrid power system with battery bank using discrete wind speed frame analysis," in *Proc. Int. Conf. Probabilistic Methods Appl. Power Syst.*, Jun. 2006, pp. 1–7.

[34] B. Bagen and R. Billinton, "Reliability cost/worth associated with wind energy and energy storage utilization in electric power systems," in *Proc. 10th Int. Conf. Probablistic Methods Appl. Power Syst.*, May 2008, pp. 1–7.

[35] J. Belhadj, "Optimal sizing of a stand-alone photovoltaic system using statistical approach," *Int. J. Renew. Energy Res.*, vol. 4, no. 2, pp. 329–337, 2014.

[36] A. Azizivahed, E. Naderi, H. Narimani, M. Fathi, and M. R. Narimani, "A new bi-objective approach to energy management in distribution Networks with energy storage systems," *IEEE Trans. Sustain. Energy*, vol. 9, no. 1, pp. 56–64, Jan. 2018.

[37] S. S. Singh and E. Fernandez, "Method for evaluating battery size based on loss of load probability concept for a remote PV system," in *Proc. 6th IEEE Power India Int. Conf. (PIICON)*, Dec. 2014, pp. 1–5.

[38] W. Zhang, A. Maleki, and M. A. Rosen, "A heuristic-based approach for optimizing a small independent solar and wind hybrid power scheme incorporating load forecasting," *J. Cleaner Prod.*, vol. 241, Dec. 2019, Art. no. 117920.

[39] A. Maleki, "Modeling and optimum design of an off-grid PV/WT/FC/diesel hybrid system considering different fuel prices," *Int. J. Low-Carbon Technol.*, vol. 13, no. 2, pp. 140–147, 2018.

[40] G. Zhang, B. Wu, A. Maleki, and W. Zhang, "Simulated annealing-chaotic search algorithm based optimization of reverse osmosis hybrid desalination system driven by wind and solar energies," *Solar Energy*, vol. 173, pp. 964–975, Oct. 2018.

[41] W. Zhang, A. Maleki, M. A. Rosen, and J. Liu, "Sizing a stand-alone solar-wind-hydrogen energy system using weather forecasting and a hybrid search optimization algorithm," *Energy Convers. Manage.*, vol. 180, pp. 609–621, Jan. 2019.

[42] A. Maleki, M. G. Khajeh, and M. Ameri, "Optimal sizing of a grid independent hybrid renewable energy system incorporating resource uncertainty, and load uncertainty," *Int. J. Elect. Power Energy Syst.*, vol. 83, pp. 514–524, Dec. 2016.

[43] A. Maleki, "Design and optimization of autonomous solar-wind-reverse osmosis desalination systems coupling battery and hydrogen energy storage by an improved bee algorithm," *Desalination*, vol. 435, pp. 221–234, Jun. 2018.

[44] P. Ralon, M. Taylor, A. Ilas, H. Diaz-Bone, and K. Kairies, "Electricity storage and renewables: Costs and markets to 2030," Int. Renew. Energy Agency, Abu Dhabi, UAE, Tech. Rep., 2017.

[45] W. Li, *Risk Assessment of Power Systems: Models, Methods, and Applications*. Hoboken, NJ, USA: Wiley, 2014.

[46] C. Grigg, P. Wong, P. Albrecht, R. Allan, M. Bhavaraju, R. Billinton, Q. Chen, C. Fong, S. Haddad, S. Kuruganty, W. Li, R. Mukerji, D. Patton, N. Rau, D. Reppen, A. Schneider, M. Shahidehpour, and C. Singh, "The IEEE reliability test system-1996. A report prepared by the reliability test system task force of the application of probability methods subcommittee," *IEEE Trans. Power Syst.*, vol. 14, no. 3, pp. 1010–1020, Aug. 1999.

[47] T. S. Brinsmead, P. Graham, J. Hayward, E. L. Ratnam, and L. Reedman, "Future energy storage trends: An assessment of the economic viability, potential uptake and impacts of electrical energy storage on the NEM 2015–2035," CSIRO, Canberra, ACT, Australia. Tech. Rep. EP155039, 2015.

[48] D. A. Douglass and A. Edris, "Real-time monitoring and dynamic thermal rating of power transmission circuits," *IEEE Trans. Power Del.*, vol. 11, no. 3, pp. 1407–1418, Jul. 1996.

[49] M. J. Brook and B. A. Finney, "Generation of bivariate solar radiation and temperature time series," *Solar Energy*, vol. 39, no. 6, pp. 533–540, 1987.

[50] R. Billinton, H. Chen, and R. Ghajar, "Time-series models for reliability evaluation of power systems including wind energy," *Microelectron. Rel.*, vol. 36, no. 9, pp. 1253–1261, 1996.

[51] H. Abunima, J. Teh, and H. J. Jabir, "A new solar radiation model for a power system reliability study," *IEEE Access*, vol. 7, pp. 64758–64766, 2019.

[52] J. Hauke and T. Kossowski, "Comparison of values of Pearson's and Spearman's correlation coefficients on the same sets of data," *Quaestiones Geographicae*, vol. 30, no. 2, pp. 87–93, 2011.

[53] D. K. Khatod, V. Pant, and J. Sharma, "Analytical approach for well-being assessment of small autonomous power systems with solar and wind energy sources," *IEEE Trans. Energy Convers.*, vol. 25, no. 2, pp. 535–545, Jun. 2010.

[54] P. K. Katti and M. K. Khedkar, "Alternative energy facilities based on site matching and generation unit sizing for remote area power supply," *Renew. Energy*, vol. 32, no. 8, pp. 1346–1362, 2007.

[55] S. M. Pandit and S.-M. Wu, *Time Series and System Analysis With Applications*, vol. 3. New York, NY, USA: Wiley, 1983.

[56] W. Wangdee and R. Billinton, "Considering load-carrying capability and wind speed correlation of WECS in generation adequacy assessment," *IEEE Trans. Energy Convers.*, vol. 21, no. 3, pp. 734–741, Sep. 2006.

[57] P. Giorsetto and K. F. Utsurogi, "Development of a new procedure for reliability modeling of wind turbine generators," *IEEE Trans. Power App. Syst.*, vol. PAS-102, no. 1, pp. 134–143, Jan. 1983.

[58] R. Billinton, J. Oteng-Adjei, and R. Ghajar, "Comparison of two alternate methods to establish an interrupted energy assessment rate," *IEEE Trans. Power Syst.*, vol. 2, no. 3, pp. 751–757, Aug. 1987.

[59] R. Hemmati, H. Saboori, and M. A. Jirdehi, "Multistage generation expansion planning incorporating large scale energy storage systems and environmental pollution," *Renew. Energy*, vol. 97, pp. 636–645, Nov. 2016.

[60] J. Santisirisomboon, B. Limmeechokchai, and S. Chungpaibulpatana, "Impacts of biomass power generation and $CO_2$ taxation on electricity generation expansion planning and environmental emissions," *Energy Policy*, vol. 29, no. 12, pp. 975–985, 2001.

[61] H. Zerriffi, H. Dowlatabadi, and A. Farrell, "Incorporating stress in electric power systems reliability models," *Energy Policy*, vol. 35, no. 1, pp. 61–75, 2007.

[62] A. Ilas, P. Ralon, A. Rodriguez, and M. Taylor, "Renewable power generation costs in 2017," Int. Renew. Energy Agency, Abu Dhabi, UAE, Tech. Rep., 2018.

[63] W. J. Cole and A. Frazier, "Cost projections for utility-scale battery storage," Nat. Renew. Energy Lab., Golden, CO, USA, Tech. Rep. NREL/TP-6A20-73222, 2019.

[64] R. Fu, T. W. Remo, and R. M. Margolis, "2018 U.S. utility-scale photovoltaics-plus-energy storage system costs benchmark," Nat. Renew. Energy Lab., Golden, CO, USA, Tech. Rep. NREL/TP-6A20-71714, 2018.

[65] M. Varadarajan and K. S. Swarup, "Solving multi-objective optimal power flow using differential evolution," *IET Gener., Transmiss. Distrib.*, vol. 2, no. 5, pp. 720–730, Sep. 2008.

[66] J. Teh and I. Cotton, "Reliability impact of dynamic thermal rating system in wind power integrated network," *IEEE Trans. Rel.*, vol. 65, no. 2, pp. 1081–1089, Jun. 2016.

[67] L. N. Kishore and E. Fernandez, "Reliability well-being assessment of PV-wind hybrid system using Monte Carlo simulation," in *Proc. Int. Conf. Emerg. Trends Elect. Comput. Technol.*, Mar. 2011, pp. 63–68.

[68] K. Deb, *Multi-Objective Optimization Using Evolutionary Algorithms*, vol. 16. Hoboken, NJ, USA: Wiley, 2001.

**FARIHAN MOHAMAD** received the B.Eng. degree (Hons.) in electrical engineering from Universiti Sains Malaysia (USM), Penang, Malaysia, in 2017, where she is currently pursuing the Ph.D. degree in electrical engineering.

She is also a Registered Engineer with the Board of Engineers Malaysia (BEM). Her research interests include energy storage systems, renewable energy, and reliability modelling of power networks.

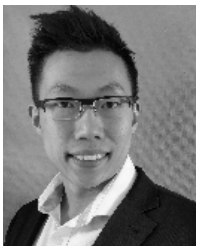

**JIASHEN TEH** received the B.Eng. degree (Hons.) in electrical and electronic engineering from Universiti Tenaga Nasional (UNITEN), Selangor, Malaysia, in 2010, and the Ph.D. degree in the similar field from the University of Manchester, Manchester, U.K., in 2016.

Since 2016, he has been a Senior Lecturer/Assistant Professor with the Universiti Sains Malaysia (USM), Penang, Malaysia. In 2018, he was appointed and served as an Adjunct Professor with the Green Energy Electronic Center, National Taipei University of Technology (Taipei Tech), Taipei, Taiwan. He is also an Adjunct Professor with the Intelligent Electric Vehicle and Green Energy Center, National Chung Hsing University (NCHU), Taichung, Taiwan. His research interests include probabilistic modelling of power systems, grid-integration of renewable energy sources, and reliability modelling of smart grid networks.

Dr. Teh is a Chartered Engineer (CEng) conferred by the Engineering Council, U.K., and The Institution of Engineering and Technology (IET), consultant for various local companies; a member of the IEEE Power and Energy Society, The Institution of Engineers Malaysia (IEM); and a Registered Engineer with the Board of Engineers Malaysia (BEM). He received the outstanding publication awards from USM, in 2017 and 2018. He is also a Regular Invited Reviewer for the *International Journal of Electrical Power and Energy Systems*, IEEE Access, the IEEE Transactions on Industry Applications, the IEEE Transactions on Vehicular Technology, the IEEE Transactions on Reliability, the IEEE Transactions on Industrial Electronics, and the *IET Generation, Transmission and Distribution*.

**HAMZA ABUNIMA** received the B.S. degree in electrical engineering from the Islamic University of Gaza, Gaza, Palestine, in 2011, and the M.Sc. degree in electrical engineering (industrial power) from the Universiti Teknikal Malaysia, Melaka, Malaysia, in 2015. He is currently pursuing the Ph.D. degree in power systems and energy conversion with the Universiti Sains Malaysia (USM), Penang, Malaysia.